文章编号：1001-9014(2019)06-0690-05

DOI:10.11972/j.issn.1001-9014.2019.06.002

Investigations on an improved transmission line for THz DNP-NMR spectroscopy

CAO Yi-Chao, CHEN Qiang, ZHANG Chen, SONG Tao, HUANG Jie, HU Qiao, LIU Di-Wei, WANG Wei*, HU Min, ZHONG Ren-Bin, SHEN Hao

(School of Electronic Science and Engineering, University of Electronic Science and Technology of China, Chengdu 610054, China)

Abstract: The improved transmission and mirror system for a 263 GHz DNP-NMR spectrometer has been designed and numerically simulated based on the geometric optics theory and the vector diffraction theory. The system includes two corrugated waveguides, a parabolic mirror and an angle-adjustable phase-correcting mirror. The simulation results show that a well-focused Gaussian-like output wave-beam with 99.90% scalar Gaussian mode content, 99.55% vector Gaussian mode content has been obtained. The direction of the output beam can be changed by only adjusting the angle of the phase-correcting mirror to match the DNP-NMR sample. The scalar Gaussian mode content is about 99.57%, and the vector Gaussian mode content is about 98.97% when the direction of the output beam changes in ± 15°.

Key words: transmission line, phase-correcting mirror, nuclear magnetic resonance, dynamic nuclear polarization.

PACS: 84.40.Az

应用于动态核极化核磁共振系统的改进型传输线研究

曹毅超, 陈 强, 张 晨, 宋 韬, 黄 杰, 胡 巧, 刘頔威, 王 维*, 胡 旻, 钟任斌, 沈 皓

(电子科学与工程学院 电子科技大学,四川 成都 610054)

摘要:基于几何光学理论和矢量衍射理论,设计了263 GHz DNP-NMR谱仪的改进反射镜系统,并进行了数值模拟.该系统包括两个波纹波导、一个抛物面镜和一个角度可调的相位校正镜.仿真结果表明,获得了聚焦良好的类高斯输出光束,其标量高斯模含量为99.90%,矢量高斯模含量为99.55%.只有通过调整相位校正镜的角度来匹配DNP-NMR样品,才能改变输出光束的方向.当输出光束方向在±15°变化时,标量高斯模含量约为99.57%,矢量高斯模含量约为98.97%.

关 键 词:传输线;相位矫正镜;核磁共振;动态核极化

中图分类号:TN814 **文献标识码**:A

Introduction

NUCLEAR magnetic resonance (NMR) allows the observation of specific quantum mechanical magnetic properties of the atomic nucleus. Many scientific techniques exploit NMR phenomena to study molecular biology, biochemistry, crystals, and non-crystalline materials through nuclear magnetic resonance spectroscopy[1-4]. However, low sensitivity and spectral resolution have been a roadblock limiting its applications. Dynamic nuclear polarization (DNP) is an NMR technique used to enhance the sensitivity through irradiation of the electron spins with electromagnetic waves in the neighborhood of

Received date: 2018-05-17, **revised date**: 2019-09-12 **收稿日期**:2018-05-17,**修回日期**:2019-09-12

Foundation items: Supported by the National Key Research and Development Program of China (2017YFA0701000), the Fundamental Research Funds for the Central Universities (A03018023601003).

Biography: CAO Yi-Chao(1994-), male, Chengdu, China, master. Research area involves terahertz technology and applications. E-mail:523647984@qq.com

*Corresponding author: E-mail: dawei@uestc.edu.cn

their Larmor frequency[5]. To obtain higher resolution spectra, modern NMR spectroscopy has pushed to much higher magnetic fields. The extension of DNP NMR to high magnetic fields depends on the development of THz sources of radiation producing few tens of watts of output power at the relevant frequencies.

Gyrotrons are the most powerful sources of radiation in the range of millimeter, sub-millimeter and terahertz waves with relatively high power levels, high stability of the output parameters, long lifetimes, and efficient scaling to higher frequency[6-9]. Solid-state devices in THz range suffer from scalability and efficiency issues that lead to limited output powers. Classical microwave tubes, e. g., traveling-wave tube (TWT) and the Extended Interaction Klystron (EIK), can produce high power (hundreds of watts) electromagnetic radiation up to 100 GHz[10]. However, these slow-wave devicesrequire physical

structures in the interaction region that is much smaller than the wavelength of operation, which produces difficulties with thermal damage and manufacturing of the interaction structure when the operation frequency is extended into THz range. Gyrotrons are the only demonstrated, highly stable devices capable of producing adequate power with an adequate lifetime in the frequency of interest for DNP NMR[11-12].

At University of Fukui in Japan, a THz gyrotron named Gyrotron FU CW VI with a 15 Tesla superconducting magnet has been developed recently. It operates at TE06 mode with a continuous frequency tuning bandwidth of approximately 1.5 GHz at 395.2 GHz[13]. This gyrotron is designed for a 600 MHz DNP-NMR spectrometer at Institute for Protein Research, Osaka University. Massachusetts Institute of Technology (MIT) has succeeded in the operation of the gyrotron at 263 GHz by using a 9.7 T magnet and operating at TE03 mode for MAS NMR experiments at ~100 K[14]. A continuous-wave (CW) tunable second-harmonic 460 GHz gyrotron was developed at MIT for 700 MHz NMR experiments[15], which operates at TE11,2 mode with a smooth frequency tuning range of 1 GHz.

For a DNP-NMR spectrometer, the power generated by the THz gyrotron should be transmitted to the sample with low loss, However, the THz gyrotrons mentioned above operate at high-order modes, which cannot be transmitted to the sample directly with low loss. A conventional transmission line for the DNP-NMR spectroscopy is shown in Fig. 1. The transmission line mainly includes: a quasi-optical mode converter converting an operating gyrotron mode into a fundamental Gaussian beam[16-17], a large-diameter corrugated waveguide used to transmit the Gaussian beam with low loss, and the mirrors which are utilized to focus the beam and match the beam from a large-diameter corrugated waveguide into a small-diameter corrugated waveguide used in the DNP-NMR probe[12,18]. In order to enhance the Gaussian beam quality radiated at the sample in a DNP-NMR spectrometer, an improved transmission line for transmitting the radiation from the THz gyrotron to the NMR probe has been proposed. In the transmission line, an angle-adjustable phase-correcting mirror is added to improve the Gaussian beam quality and adjust the direction of output beam.

This paper is organized as follows. Section 1 presents the design of the improved transmission line. The numerical calculation results and discussions are presented in Section 2. Section 3 is the summary and conclusions.

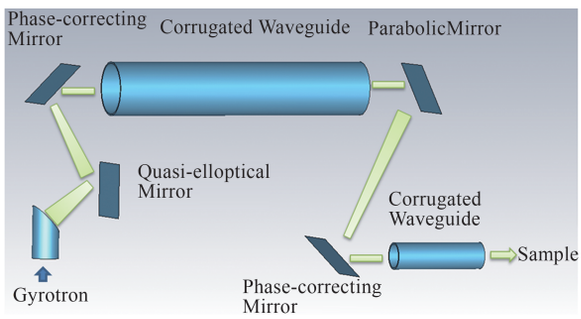

Fig. 1　The layout of the transmission-line for DNP-NMR spectroscopy
图 1　DNP-NMR 谱仪传输线的布置

1　Design of the transmission line

The structure of the improved transmission line for a 263 GHz gyrotron in the 400 MHz DNP-NMR spectrometer is shown in Fig. 2(a). The system consists of two metallic corrugated waveguides, an angle-adjustable phase-correcting mirror and a parabolic mirror. A Gaussian beam from the Quasi-optical mode converter, as the input of the transmission line, is radiated into a 22 mm diameter metallic corrugated waveguide in which the depth, the width and the period of the corrugation are 0.285 mm, 0.253 mm and 0.38 mm, respectively.

The beam from the 22 mm diameter corrugated waveguide is focused with the parabolic mirror, and the phase-correcting mirror is used to correct the amplitude and phase distributions of the outgoing wave beam to improve the Gaussian beam content of the beam at the sample. The phase-correcting mirror is shown in Fig. 2(b). These mirrors also match the beam size from the 22 mm corrugated waveguide into the 8mm corrugated waveguide used in the NMR probe.

The vector diffraction theory of electromagnetic waves is utilized to analysis this process[19]. The Stratton-Chu formula presented as follows can be used to calculate the vector diffraction fields E' and H' at the observing point P(x′, y′, z′) when the source fields E and H are known.

$$\mathbf{E}' = \oint_S j\omega\mu(\mathbf{n}\times\mathbf{H})G\mathrm{d}S + \oint_S \left[(\mathbf{n}\cdot\mathbf{E})\nabla G + (\mathbf{n}\times\mathbf{E})\times\nabla G\right]\mathrm{d}S, \quad (1)$$

$$\mathbf{H}' = -\oint_S j\omega\varepsilon(\mathbf{n}\times\mathbf{E})G\mathrm{d}S + \oint_S \left[(\mathbf{n}\cdot\mathbf{H})\nabla G + (\mathbf{n}\times\mathbf{H})\times\nabla G\right]\mathrm{d}S, \quad (2)$$

where G is the Green function for a point source in the

free space.

$$G = \frac{e^{-jk_0R}}{4\pi R} \quad , \quad (3)$$

where R is the distance between the source point Q (x, y, z) and the observing point P (x', y', z'), k_0 is the wave number in free space.

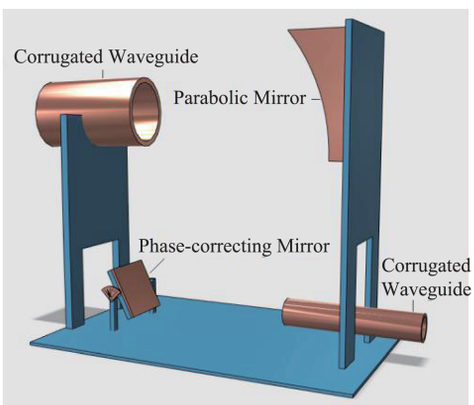

(a)

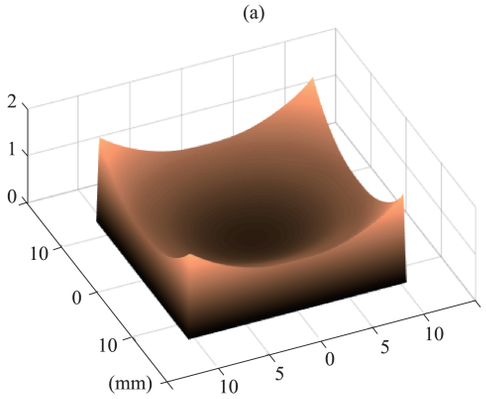

(b)

Fig.2 (a) Sketch of the improved transmission and mirror system, and (b) Shape of the phase-correcting mirror
图2 (a)改进的透射镜和反射镜系统的结构,(b)相位校正镜的形状

The principle of the phase-correcting mirror is shown in Fig. 3. To obtain the phase of the corrected and adjusted field $u_m(\vec{r})$, the original incident beam field $u(\vec{r})$ at the mirror is multiplied by a phase term

$$u_m(\vec{r}) = u(\vec{r})e^{j2k_0\Delta z(\vec{r})\cos\alpha} \quad , \quad (4)$$

here, $\vec{r}$ is the position vector of the mirror surface, $\Delta z(\vec{r})$ is the surface deformation of the mirror, and α is the angle of the incidence or the reflection wave. The phase-correcting mirror is optimized through the iteration formula as follows [20].

$$\Delta z^{i+1}(\vec{r}) = \frac{1}{2k_0\cos\alpha}\left[\frac{\pi}{2} - \arg\left(j2k_0u(\vec{r})q^i(\vec{r})\cos\alpha\right)\right], \quad (5)$$

$$q^i(\vec{r}) = -4\iint_{S_0}\left(u_g(\vec{r}_0) - u_r^i(\vec{r}_0)\right)^* \frac{\partial}{\partial z}G(\vec{r}_0 - \vec{r})\,dx_0dy_0, \quad (6)$$

$$G(\vec{r}_0 - \vec{r}) = \frac{\exp\left(-jk_0(\vec{r}_0 - \vec{r})\right)}{4\pi\left|\vec{r}_0 - \vec{r}\right|} \quad , \quad (7)$$

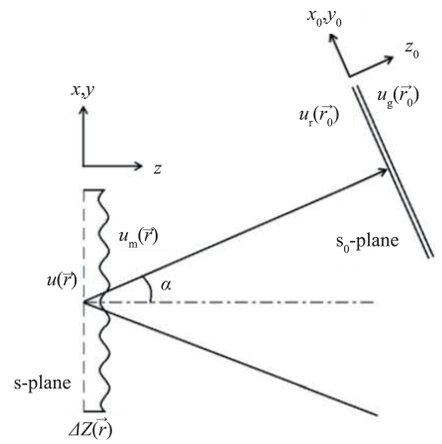

Fig. 3 Principle of the phase-correcting method
图3 相位矫正原理

where, G is the Green function, the superscript "*" represents the complex conjugate, $u_r(\vec{r}_0)$is the field distribution of the wave beam at $\vec{r}_0$, and $u_g(\vec{r}_0)$ is the desired field distribution.

The scalar Gaussian mode content correlation coefficient $\eta_s$and the vector Gaussian mode content correlation coefficient $\eta_v$are usually used to describe the mode purity of the output beam, which are defined as the amplitude and phase correlation coefficient of fields to an ideal fundamental Gaussian distribution [21-22].

$$\eta_s = \left(\iint_S |u_1|\cdot|u_2|\,dS\right)/\sqrt{\iint_S|u_1|^2dS\cdot\iint_S|u_2|^2dS}, \quad (8)$$

$$\eta_v = \left|\iint_S u_1\cdot u_2^*dS\right|^2/\left(\iint_S|u_1|^2dS\cdot\iint_S|u_2|^2dS\right). \quad (9)$$

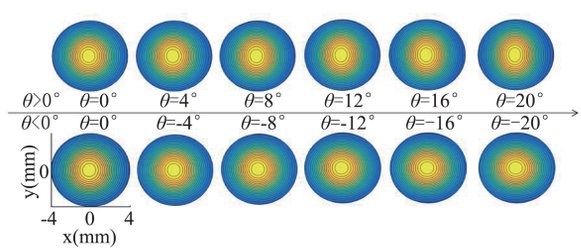

Fig. 4 Normalized power distribution of the output field versus the angle of the phase-corrected mirror(Plotted by Matlab)
图4 输出场与相位校正镜角度的归一化功率分布(Matlab计算的结果)

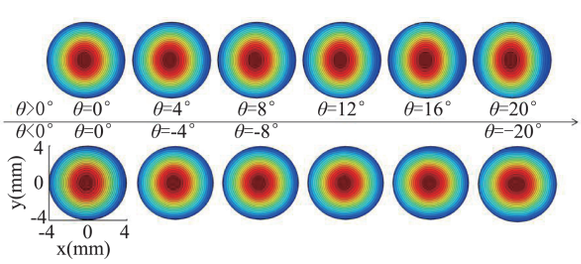

Fig. 5 Normalized power distribution of the output field versus the angle of the phase-corrected mirror(Plotted byFEKO)
图5 输出场的归一化功率分布与相位校正镜的角度(FEKO计算结果)

2 Numerical calculation results

Based on the design and analytic method of the transmission line in Section 1, the beam field distribution at the output window is calculated with Matlab. The normalized power distribution at the output window with the angular adjustment of the phase-correcting mirror is shown in Fig. 4, and the result calculated by FEKO is in Fig. 5. FEKO is a 3D full wave electromagnetic simulation software. Since the MoM is used, FEKO does not need to set boundary conditions during simulation. It is found that the beam can keep high fundamental Gaussian mode content when the direction of the output wave-beam changes within ± 20°. When the angle of the phase-correcting mirror is 0°, the scalar Gaussian mode content is 99. 90%, the vector Gaussian mode content is 99. 55%, the efficiency is up to 96. 20%, and the beam waist is 3. 01 mm at the window plane, as shown in Table 1. The results calculated by FEKO at the angle of 0° are listed in Table 2.

The direction of the output beam can be changed by only adjusting the angle of the phase-correcting mirror to match the DNP-NMR sample. As shown in Fig. 6, when the direction of the output beam change from -15° to 15°, the scalar and the vector Gaussian mode content at the output window always keep 99. 70% ± 0. 2% and 99. 3% ± 0. 2%, respectively. The electric field distribution at the cross section of the improved transmission line from a 3D simulation software FEKO is presented in Fig. 7.

Table 1　Matlab results
表 1　Matlab 结果

Scalar Gaussian mode content	99. 90%
Vector Gaussian mode content	99. 55%
Effeciency	96. 20%
Waist radius	3. 01 mm

Table 2　FEKO Results
表 2　FEKO 结果

Scalar Gaussian mode content	99. 83%
Vector Gaussian mode content	99. 44%
Efficiency	95. 65%
Waist radius	3. 00 mm

3 Conclusion

The improved transmission and mirror system for a 263 GHz DNP-NMR spectrometer have been designed and numerically simulated in this paper based on the geometric optics theory and the vector diffraction theory. Numerical calculations and the results of FEKO show the phase-correcting mirror added in the improved transmission line can improve the scalar and vector Gaussian mode contents of the output beam. When the angle of the phase-correcting mirror is 0°, the scalar and vector Gaussian mode content are 99. 90% and 99. 55%, respectively. Meanwhile, the direction of the output beam can be changed by only adjusting the angle of the angle-adjustable phase-correcting mirror. The scalar Gaussian mode content is about 99. 57% and the vector Gaussian mode content is about 98. 97% when the direction of the output beam changes within ± 15°. This improved transmission and mirror system give an efficient solution to the problem of transmission for a 400 MHz DNP-NMR spectrometer.

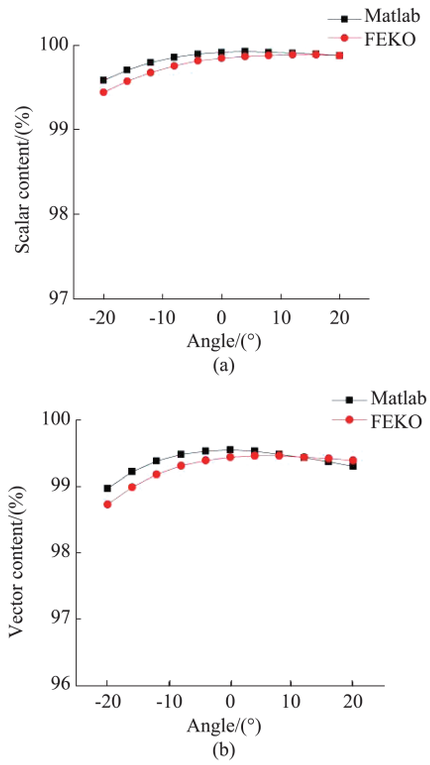

Fig.6　(a) The scalar Gaussian mode content versus. angle of the phase-corrected mirror, and (b) the vector Gaussian mode content vs. angle of the phase-corrected mirror
图 6　(a)标量高斯成分与相位校正镜角度关系,(b)矢量高斯成分与相位校正镜角度关系

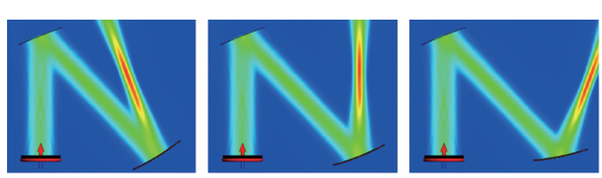

Fig. 7　The electric field distribution of the cross section of the improved transmission line from 3-D simulation software FEKO with: (a) 20°, (b) 0°, and (c)-20°
图 7　用 FEKO 三维模拟软件计算改进后的输电线路截面电场分布(a)20°,(b)0°,(c)-20°

References

[1] Markley J L, Bruschweiler R, Edison A S, *et al*. The future of NMR-based metabolomics [J]. *Current Opinion in Biotechnology*, 2017, **43**:34-40..
[2] Fan T W M, Lane A N. Applications of NMR spectroscopy to systems biochemistry [J]. *Progress in Nuclear Magnetic Resonance Spectroscopy*, 2016, **92-93**:18-53.
[3] Andreas L B, Le MarchandT, Jaudzems K, *et al*. High-resolution proton-detected NMR of proteins at very fast MAS [J]. *Journal of Magnetic Resonance*, 2015, **253**:36-49.

[4] Pecher O, Carretero-Gonzalez J, Griffith K J, *et al*. Materials' methods: NMR in battery research [J]. *Chemistry of Materials*, 2017, **29**(1): 213-242.
[5] Hall D A, Maus D C, Gerfen G J, *et al*. Polarization-enhanced NMR spectroscopy of biomolecules in frozen solutions [J]. *Science*, 1997, **276**(5314):930-932.
[6] Liu S G, Yuan X S, Fu W J, *et al*. The coaxial gyrotron with two electron beams. I. Linear theory and nonlinear theory [J]. *Physics of Plasmas*, 2007, **14**(10):.103113-1-7.
[7] Liu D W, Wang W, Qiao S, *et al*. Study of a coaxial gyrotron cavity with improved mode selection [J]. *IEEE Transactions on Electron Devices*, 2013, **60**(12):4248-4251.
[8] Idehara T, Ogawa I, Agusu L, *et al*. Development of 394.6 GHz CW gyrotron (gyrotron FU CW II) for DNP/Proton-NMR at 600 MHz [J]. *International Journal of Infrared and Millimeter Waves*, 2007, **28**(6):433-442.
[9] Hornstein M K, Bajaj V S, Griffin R G, *et al*. Second harmonic operation at 460 GHz and broadband continuous frequency tuning of a gyrotron oscillator [J]. *IEEE Transactions on Electron Devices*, 2005, **52**(5):798-807.
[10] Roitman A, Berry D, Steer B. State-of-the-art W-band extended interaction klystron for the CloudSat program [J]. *IEEE Transactions on Electron Devices*, 2005, **52**(5):895-898.
[11] Blank M, Borchard P, Cauffman S, *et al*. High-frequency gyrotrons for DNP-enhanced NMR applications [C] *IEEE International Vacuum Electronics Conference*, 2014, pp.7-8.
[12] Nanni E A, Barnes A B, Griffin R G, *et al*. THz dynamic nuclear polarization NMR [J]. *IEEE Transactions on Terahertz Science and Technology*, 2011, **1**(1):145-163.
[13] Idehara T, Kosuga K, Agusu L, *et al*. Continuously frequency tunable high power sub-THz radiation source—gyrotron FU CW VI for 600 MHz DNP-NMR spectroscopy [J]. *Journal of Infrared, Millimeter, and Terahertz Waves*, 2010, **31**(7):775-790.
[14] Rosay M, Tometich L, Pawsey S, *et al*. Solid-state dynamic nuclear polarization at 263 GHz: spectrometer design and experimental results [J]. *Physical Chemistry Chemical Physics*, 2010, **12**(22): 5850-5860.
[15] Torrezan A C, Han S, Mastovsky I, *et al*. Continuous-wave operation of a frequency-tunable 460-GHz second-harmonic gyrotron for enhanced nuclear magnetic resonance [J]. *IEEE Transactions on Plasma Science*, 2010, **38**(6):1150-1159.
[16] Wang W, Liu D W, Qiao S, *et al*. Study on the terahertz denisov quasi-optical mode convertor [J]. *IEEE Transactions on PlasmaScience*, 2014, **42**(2):346-349.
[17] Wang W, Song T, Shen H, *et al*. Quasi-optical mode converter for a 0.42 THz TE17,4 mode pulsed gyrotron oscillator [J]. *IEEE Transactions on Electron Devices*, 2017, **64**(4):1751-1755.
[18] Woskov P P, Bajaj V S, Hornstein M K, *et al*. Corrugated waveguide and directional coupler for CW 250-GHz gyrotron DNP experiments [J]. *IEEE Transactions on Microwave Theory and Techniques*, 2005, **53**(6):1863-1869.
[19] Stratton J A. *Electromagnetic Theory* [M]. New York, NY, USA: Mcgraw- Hill, 1941, pp. 424-468.
[20] Yang X, Thumm M K, Arnold A, *et al*. Progress toward optimization of phase-correcting mirrors for a multifrequency 1-MW gyrotron [J]. *IEEE Transactions on Plasma Science*, 2006, **34**(3):652-658.
[21] Liu J, Jin J, Thumm M, *et al*. Vector method for synthesis of adapted phase-correcting mirrors for gyrotron output couplers [J]. *IEEE Transactions on Plasma Science*, 2013, **41**(9):2489-2495.
[22] Goldsmith P F. *Quasioptical Systems: Gaussian Beam Quasioptical Propagation and Applications 1st ed* [M]. New York, NY, USA: Wiley, 1998, ch. 2.